RSC Advances

PAPER

View Article Online
View Journal | View Issue

Cite this: *RSC Adv.*, 2026, **16**, 23974

Sustainable deep eutectic solvent-engineered clove-derived carbon dots as a single sensing platform for the detection of multiple antioxidants

Mandeep Kaur,† Mallika Phull,† Urvashi Singh, Diksha Bhatia and Banibrata Maity *

Antioxidants are essential for mitigating oxidative stress and preserving cellular homeostasis, underscoring the need for sustainable, analytically robust detection platforms. Here, we propose an environmentally friendly and effective method for producing fluorescent carbon dots (CDs) from clove (Syzygium aromaticum) under hydrothermal conditions utilizing a deep eutectic solvent (choline chloride and urea). This ecologically friendly method eliminates the need for harmful reagents and produces very uniform CDs with an average particle size of ~2.1 nm and a fluorescence quantum yield of 22.5%. Detailed structural and compositional investigations employing HR-TEM, FT-IR, and XPS reveal effective carbonization as well as the presence of several surface functional groups that contribute to the excellent optical characteristics. The as-prepared CDs show excitation-dependent fluorescence emission, outstanding photostability, and remarkable stability throughout a wide pH, ionic strength, and irradiation time range. With low detection limits of 0.25 μM and 0.14 μM, respectively, the CDs are extremely sensitive and selective fluorescent nanoprobes for quercetin (QT) and riboflavin (RF). The improved sensing performance is ascribed to the effective interactions between the analytes and the surface functionalities of the CDs. Overall, this study demonstrates how deep eutectic solvent engineering and biomass-derived precursors may work together to create functional nanomaterials in a sustainable manner. The proposed CDs have considerable potential for use in antioxidant sensing as well as in extensive bioanalytical and environmental monitoring systems.

Received 13th March 2026
Accepted 29th April 2026

DOI: 10.1039/d6ra02145j

rsc.li/rsc-advances

1 Introduction

The development of environmentally benign solvents is a pivotal focus in green chemistry.[1] The continuous accumulation of hazardous chemical waste, coupled with rising environmental concerns, has intensified the search for sustainable alternatives to conventional solvents. In this context, deep eutectic solvents (DESs) have emerged as a promising class of green solvents, offering a viable substitute for traditional toxic solvents, including ionic liquids.[2] They are typically synthesized by combining a quaternary ammonium salt with a metal salt or a hydrogen bond donor (HBD).[3] The substantial depression in melting point relative to the individual constituents arises from charge delocalization facilitated by hydrogen bonding interactions, such as those between halide anions and hydrogen-donor moieties. Due to their structural versatility, facile preparation, and the absence of purification requirements, DESs have garnered significant attention in recent years.[4] Aligned with the principles of green chemistry, their utilization aims to eliminate hazardous raw materials, reduce waste generation, and minimize energy consumption in material synthesis, without compromising the desired physicochemical properties. Despite these benefits, the translation of DESs into high-performance nanomaterial production and sensing applications is still limited, necessitating solutions that combine sustainability and functional efficiency.

In recent years, environmentally benign deep eutectic solvents DESs have attracted increasing attention as sustainable media for the "green" synthesis of nanoparticles (NPs). DESs represent a promising alternative to conventional organic and inorganic solvents owing to their low toxicity, cost-effectiveness, and environmental compatibility.[5] Over the past decade, DESs have been successfully employed across diverse synthetic domains, including nanoparticle fabrication. Among various nanostructures, carbon dots (CDs) have attracted significant attention owing to their unique optical properties, low fabrication cost, and diverse applications in sensing, bioimaging, and optoelectronics. The use of DESs in CD synthesis offers multiple benefits, such as enhanced precursor solubility, tunable surface functionalization, and environmentally benign reaction

Department of Chemistry and Biochemistry, Thapar Institute of Engineering and Technology, Patiala, 147004, India. E-mail: Banibrata.maity@thapar.edu; mkaur3_phd19@thapar.edu; phullmallika96@gmail.com; uurvashi_phd24@thapar.edu; dikshabhatia156@gmail.com

† Both authors have contributed equally.

conditions, thereby overcoming several limitations associated with traditional approaches like co-precipitation, sol–gel, and solvothermal methods.[6–8] Consequently, integrating DESs into the synthesis of CDs not only aligns with the principles of green chemistry but also facilitates the development of next-generation luminescent nanostructures with superior performance.[9–11]

Carbon dots (CDs) are modern carbon nanomaterials with sizes below 10 nm and exhibit stable physical and chemical properties. Their environmental compatibility, low toxicity, and excellent biocompatibility make them highly promising for applications in sensing devices, fluorescence imaging, and drug delivery systems.[12] CDs can be synthesized by various techniques, including laser ablation, pyrolysis, solvothermal, arc discharge, and hydrothermal methods, with the hydrothermal route considered the most straightforward and sustainable. Recent studies have emphasized improving the tunability of CDs through controlled synthesis, with particular attention to "green" methods that employ renewable natural precursors. Such approaches minimize the use of hazardous reagents and enable the sustainable production of CDs.[13] Clove buds (*Syzygium aromaticum*), a rich natural carbon source cultivated primarily in southern India, have been explored as effective precursors for green synthesis of CDs. In addition to their traditional medicinal uses, clove-derived CDs exhibit promising optical properties, reinforcing the potential of biomass-based nanomaterials within the framework of sustainable nanotechnology. Clove (*Syzygium aromaticum*) was selected as a precursor owing to its substantial phenolic constituents, particularly eugenol, which offers appropriate carbon and oxygen functionalities for the synthesis of highly fluorescent CDs. Its aromatic structure helps with carbonization and the formation of graphitic domains, which improves the optical properties and gives it a high quantum yield. Natural heteroatoms make it possible to passivate surfaces *in situ*, which increases photostability without the need for outside dopants. It also works well with deep eutectic solvents, which makes the synthesis process more efficient and environmentally friendly.[14]

Fluorescence sensing with CDs offers a rapid, sensitive, and cost-effective alternative to conventional food analysis techniques such as GC-MS and LC-MS, which, while accurate, are limited by complexity, expense, and long analysis times.[15,16] CDs provide a powerful platform for antioxidant detection and food safety monitoring, advancing research in nutrition and functional foods.[17] CDs are photoluminescent carbon nanomaterials that emit fluorescence upon excitation, with emission profiles that can be modulated either quenched or enhanced in the presence of specific analytes.[18,19] Owing to their well-defined and often linear fluorescence response to quencher concentration within a defined dynamic range, CDs have emerged as promising optical sensing platforms. Their appeal further derives from the availability of abundant precursors, operationally simple synthetic routes, and inherent biocompatibility. Nevertheless, selectively detecting multiple analytes using a single CDs platform is still a big problem, especially when different analytes need different sensing methods. It is important to fix this problem so that CD-based tools can be used in real-world scientific situations.

Li *et al.* designed a sensitive and economical voltammetric sensor to measure baicalein in herbal medicine.[20] Shi *et al.* proposes an effective and simple process for producing biomass-derived porous carbon compounds and exhibits their potential use in supercapacitors.[21] Cui *et al.* utilized microwave irradiation as an effective approach for functional lignin modification, with the goal of increasing the anti-aging characteristics of lignin-modified asphalt.[22]

Fluorescence-based analytical methods are particularly attractive in food monitoring applications due to their rapid response, high sensitivity, cost-effectiveness, and straightforward implementation.[23–25] In this context, antioxidants have attracted considerable scientific interest due to their roles in mitigating oxidative stress and conferring anti-aging and anti-inflammatory benefits. Within food systems, antioxidants are routinely incorporated to enhance stability and nutritional value, thereby stimulating growing interest in the identification and quantification of antioxidant species in natural products and food matrices.[26]

Among dietary antioxidants, flavonoids and vitamins play a central role in disease prevention and health promotion. Quercetin ($C_{15}H_{10}O_7$), the most abundant natural flavonoid, exhibits antioxidant, antiviral, anti-inflammatory, and anticancer activities, making it a valuable target for sensitive analytical detection.[27,28] Likewise, riboflavin (Vitamin B_2) is an essential micronutrient whose deficiency leads to severe physiological disorders, underscoring the importance of accurate quantification in food and pharmaceutical products.[29–31] Fluorescence-based analytical strategies, particularly those employing carbon dot (CD) platforms, thus represent a compelling approach for the selective and sensitive detection of quercetin (QT) and riboflavin (RF), enabling precise nutritional evaluation and facilitating therapeutic monitoring in complex biological and food matrices.

In this study, a facile, eco-friendly hydrothermal route was employed to synthesize carbon dots (CDs) from *Syzygium aromaticum* (clove) using a deep eutectic solvent (DES) composed of choline chloride and urea (1 : 1 molar ratio). Unlike traditional CDs synthesis methods, which need harsh chemicals, multi-step processing, or external dopants, the current work adopts a DES-assisted one-step procedure with clove as a phenolic-rich biomass precursor, allowing for simultaneous carbonization and surface functionalization. Notably, the produced CDs demonstrate dual-analyte sensing *via* different IFE and FRET processes, with extremely low limit of detection values, which is uncommon in DES-based systems, emphasizing the approach's uniqueness and functional adaptability.[32,33]

To the best of our knowledge, this is the first report of biomass-derived CDs in a DES system for application as a fluorescence sensing probe for dual antioxidant detection. The novel idea about this work is that it combines a biomass-derived precursor (clove) with DES-assisted hydrothermal method to make highly fluorescent CDs. The proposed strategy allows for carbonization and *in situ* surface functionalization to happen at the same time in a single step and under green conditions. This

is different from traditional methods that use toxic reagents or require multiple steps to passivate the surface. Additionally, the synthesized CDs demonstrate multiple-analyte sensing capability for QT and RF through two separate quenching mechanisms (IFE and FRET). The detection limits of the analytes were within the micromolar range, and applicability was validated in real matrices, including apple juice (QT) and vitamin B_2 supplements (RF). These findings underscore the potential of DES-derived CDs as sustainable and versatile nanoprobes for practical food and pharmaceutical analysis. Overall, this study not only offers sustainable method for CDs synthesis, but it also develops a performance-driven sensing platform, broadening the functional scope of DES-derived nanomaterials in analytical chemistry.

2 Experimental section

2.1 Materials and reagents

Choline chloride, urea, quinine sulfate, and metal salts [$MgCl_2$, $NiCl_2$, $Cr(NO_3)_3$, $MnCl_2$, $Pb(NO_3)_2$, $BaCl_2$, $CoCl_2$, NH_4Cl, $CuCl_2$] were purchased from Loba Chemie (India) without any further purification. Riboflavin, quercetin, and amino acids (Ala, Arg, Asn, Asp, Cys, Glu, Gln, His, Ile, Leu, Lys, Met, Thr, Trp, Tyr, Val) were obtained from Sigma-Aldrich, India. Ascorbic acid, creatinine, tetracycline, and dopamine were purchased from HiMedia Laboratories, India. Floral cloves were procured from a local grocery store in Patiala, Punjab, thoroughly washed, dried, ground into powder, and subsequently used as the carbon source for the preparation of CDs. Ultrapure deionized water was used for all stock solutions. For real-sample validation, QT was extracted from apples, and RF was extracted from commercial multivitamin supplements (Patiala, India).

2.2 Synthesis of choline chloride–urea DES

A deep eutectic solvent (DES) was synthesized by combining choline chloride (13.96 g) and urea (6.00 g) in a 1 : 1 molar ratio. The mixture was heated to 100 °C under continuous magnetic stirring for 30 min, yielding a clear, homogeneous liquid. The resulting stable green solvent was stored in a sealed glass vial and subsequently employed for the synthesis of CDs.

2.3 DES-mediated hydrothermal synthesis of CDs

CDs were synthesized through a sustainable hydrothermal strategy utilizing clove powder as a renewable carbon precursor and a DES as a green reaction medium. Clove, a widely available and non-toxic biomaterial, was selected owing to its high polyphenolic content, which facilitates carbonization and surface passivation during hydrothermal treatment. An aqueous clove extract was prepared by dispersing 500 mg of clove powder in 10 mL of deionized water, followed by ultrasonication for 2 h to ensure complete dissolution of bioactive constituents. To integrate the advantages of DES-assisted synthesis, 4 mL of the clove extract was homogeneously mixed with 4 mL of the prepared DES and subsequently transferred into a Teflon-lined stainless-steel autoclave. The mixture was subjected to hydrothermal treatment at 300 °C for 4 h, during which the synergistic effect of the DES promoted efficient carbonization under mild, environmentally benign conditions. Upon natural cooling to room temperature, a dark brown dispersion indicative of CD formation was obtained. The suspension was centrifuged at 8500 rpm for 20 min to remove larger aggregates, and the supernatant was further purified using a 0.22 μm hydrophilic membrane filter, affording a stable, clear colloidal solution of fluorescent CDs. The green, DES-assisted methodology thus provides a facile, low-cost, and non-toxic route for producing

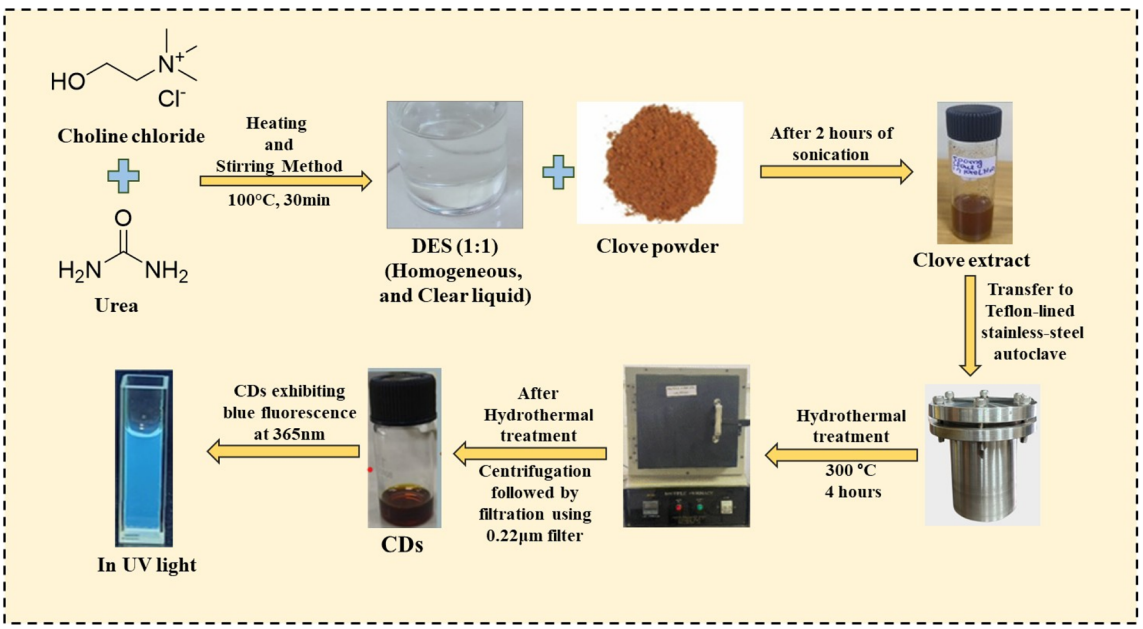

Scheme 1 Schematic representation of the hydrothermal synthesis of carbon dots (CDs) from clove powder using a choline chloride–urea-based deep eutectic solvent (DES) as a ecofriendly reaction medium.

highly stable CDs, highlighting its potential as a sustainable alternative to conventional synthetic approaches. A schematic overview of the synthetic process is depicted in Scheme 1.

2.4 Optimization of synthetic parameters for highly fluorescent CDs

The synthesis duration was found to play a significant role in governing the surface state evolution and fluorescence characteristics of the CDs. Accordingly, CDs were synthesized over varying reaction times (2–8 h), among which the sample obtained after 4 h exhibited the highest fluorescence intensity (Fig. S1a). This optimal duration is likely associated with sufficient carbon core nucleation and stabilization of surface passivation layers, which collectively enhance radiative recombination pathways. In parallel, precursor volume was optimized to maximize the nanoprobe's photoluminescence response and sensing efficiency. Systematic variation of aliquot volumes (10–50 μL) of CD stock solution introduced into 3 mL of double-distilled water revealed a pronounced intensity maximum at 10 μL (Fig. S1b). This observation suggests an optimal dispersion regime, wherein excessive particle concentration is avoided, thereby minimizing self-quenching and maximizing light–matter interaction.

2.5 Determination of photoluminescence quantum yield (Φ) and time-resolved fluorescence average lifetime (τ_{avg})

The photoluminescence quantum yield (Φ) of the CDs was determined using a relative method with quinine sulfate in 0.1 M H_2SO_4 ($\Phi_R = 0.546$) as the reference standard, under excitation at 340 nm. The value of the CDs was calculated according to the following relation:[34]

$$\Phi_S = \Phi_R \times \frac{A_S}{A_R} \times \frac{(\mathrm{Abs})_R}{(\mathrm{Abs})_S} \times \frac{(\eta_S)^2}{(\eta_R)^2} \quad (1)$$

In this equation, the subscripts 'S' and 'R' correspond to the sample (CDs) and the reference (quinine sulfate), respectively. 'Φ_S'and 'Φ_R' denote the quantum yields of the sample and reference, while 'A_S' and 'A_R' represent the integrated photoluminescence emission areas. "Abs" refers to the absorbance at the excitation wavelength, and 'η' is the refractive index of the solvent.

3 Results and discussions

3.1 Structural and compositional characterization of CDs

The particle size distribution of the synthesized CDs was determined from HRTEM images using ImageJ by analyzing a statistically significant number of particles. The analysis confirmed that the as-synthesized CDs possess a uniform spherical morphology with excellent dispersion (Fig. 1a). As shown in Fig. 1b, the CDs exhibit a narrow size distribution with an average diameter of 2.1 nm, indicating good monodispersity. The uniform dispersion of particles observed across multiple micrographs further supports the consistency of the synthesized nanodots. Surface functional groups were identified by FT-IR spectroscopy (Fig. 1c), which displayed characteristic bands at 3307 cm^{-1} (–O–H/–N–H stretching), 2912 cm^{-1} (–C–H

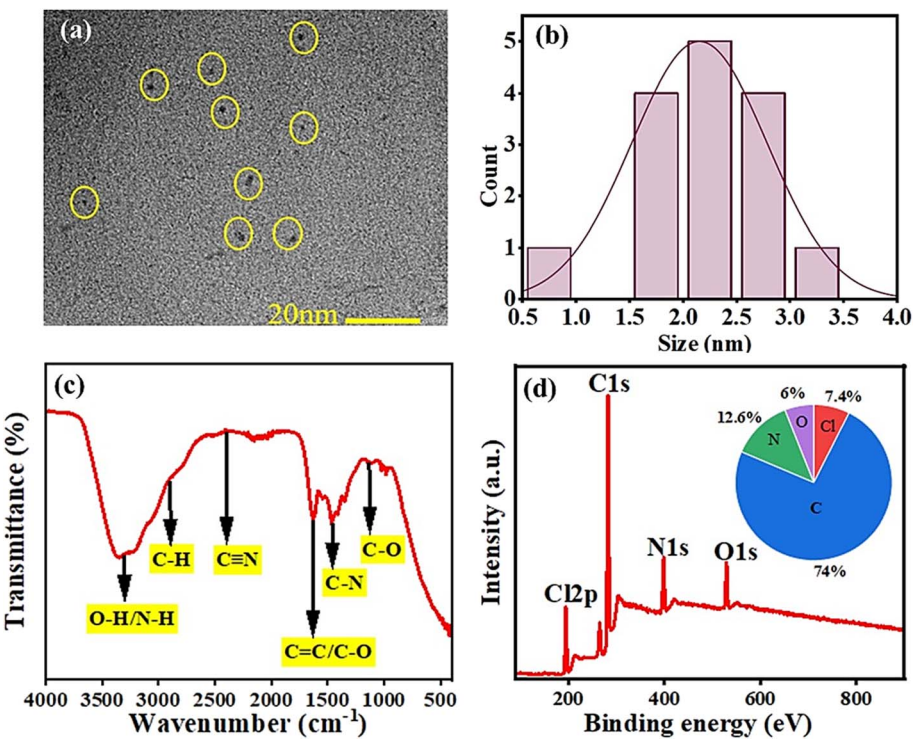

Fig. 1 (a) HR-TEM image of CDs (scale bar: 20 nm), (b) CDs particle size distribution histogram, (c) FT-IR spectrum, and (d) XPS survey spectrum of the synthesized CDs.

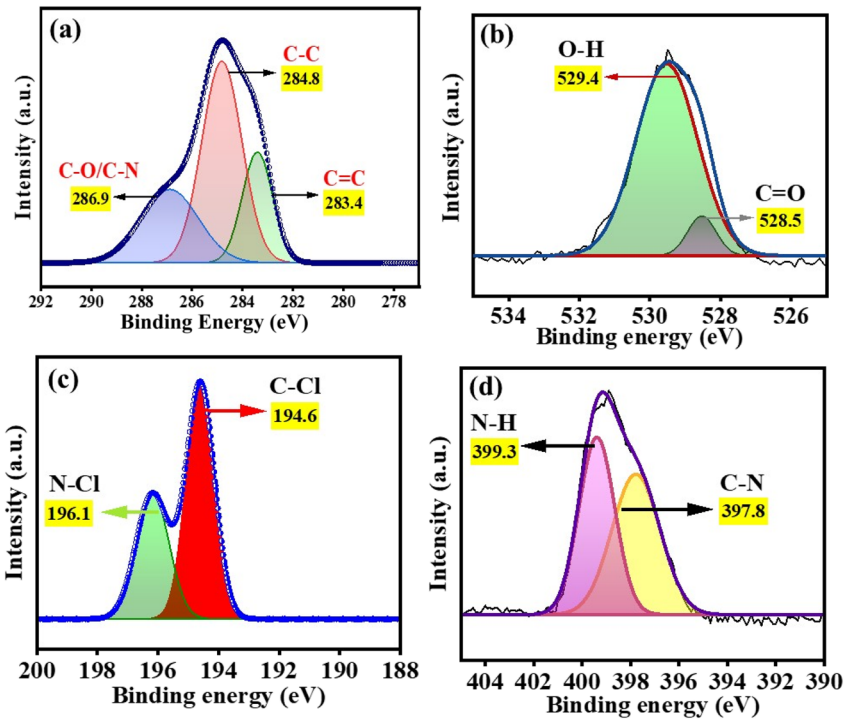

Fig. 2 Deconvoluted high-resolution XPS spectra of CDs for (a) C 1s, (b) O 1s, (c) Cl 2p, and (d) N 1s regions.

stretching), 2401 cm^{-1} (–C≡N stretching), and 1607 cm^{-1} (–C=C/–C=O stretching).[35,36] Additional peaks at 1459 cm^{-1} and 1132 cm^{-1} were assigned to –C–N and –C–O stretching vibrations, respectively.[37]

X-ray photoelectron spectroscopy (XPS) was used to determine the elemental composition and bonding environments of the synthesized CDs. The survey spectrum (Fig. 1d) displayed four distinct peaks corresponding to C 1s (282.6 eV), N 1s (398.7 eV), O 1s (528.9 eV), and Cl 2p (195.2 eV). Quantitative analysis indicated atomic compositions of C (74.0%), N (12.6%), O (6.0%), and Cl (7.4%). High-resolution C 1 s spectra (Fig. 2a) were deconvoluted into three major components at 283.4, 284.8, and 286.9 eV, assignable to the C=C, C–C, C–N/C–O bonds, respectively. The O 1s spectrum (Fig. 2b) showed peaks at 528.5 and 529.4 eV, attributed to O–H and C=O functionalities, respectively. The Cl 2p spectrum (Fig. 2c) revealed two peaks at 194.6 and 196.1 eV, corresponding to C–Cl and N–Cl species. Similarly, the N 1s spectrum (Fig. 2d) showed components at 397.8 and 399.3 eV, confirming the presence of C–N and N–Cl bonding environments.[3,33] The coexistence of C, N, O, and Cl in the CDs was further corroborated by energy-dispersive X-ray spectroscopy (EDS, Fig. S1c).

3.2 Optical characteristics of CDs

The optical characteristics of the CDs were systematically probed by UV-vis absorption and fluorescence emission spectroscopy. The UV-vis spectrum (Fig. 3a) exhibits a pronounced absorption peak at 321 nm, ascribed to the π–π* transitions within the sp^2-hybridized carbon core, accompanied by a weaker shoulder around 400 nm, indicative of n–π* transitions arising from heteroatom (N, Cl) functionalization. The aqueous CDs solution appeared pale yellow under ambient light and emitted intense blue emission under 365 nm UV irradiation (inset, Fig. 3a).[38]

CDs demonstrated excitation wavelength-dependent emission spectra in aqueous media, with maximum emission intensity at 417 nm following excitation at 340 nm (Fig. 3b). The fluorescence emission of CDs arises from the process of photoinduced charge separation and subsequent entrapment at the surface, leading to radiative recombination between hole and electron pairs.[39] The fluorescence emission of CDs exhibited a notable excitation-dependent red-shifting from 417 to 500 nm as the excitation wavelength increased from 340 to 420 nm (Fig. 3c). The excitation-dependent emission characteristic of CDs can be attributed to various factors, including the quantum confinement effect, zigzag sites, surface defects, aromatic structure formation on the surface, diverse functional groups on CDs surface, and non-uniform particle distribution.[40–42]

3.3 Environmental resilience of the nanosensor

The environmental stability of the nanosensor was systematically investigated to evaluate its potential for practical applications under diverse conditions. Specifically, the photophysical properties of the CDs, including fluorescence intensity and emission profile, were monitored as a function of pH, ionic strength, and storage duration.

3.3.1 Impact of pH and ionic strength on the performance of CDs. The stability of the prepared CDs was systematically evaluated by examining the effects of pH and ionic strength on

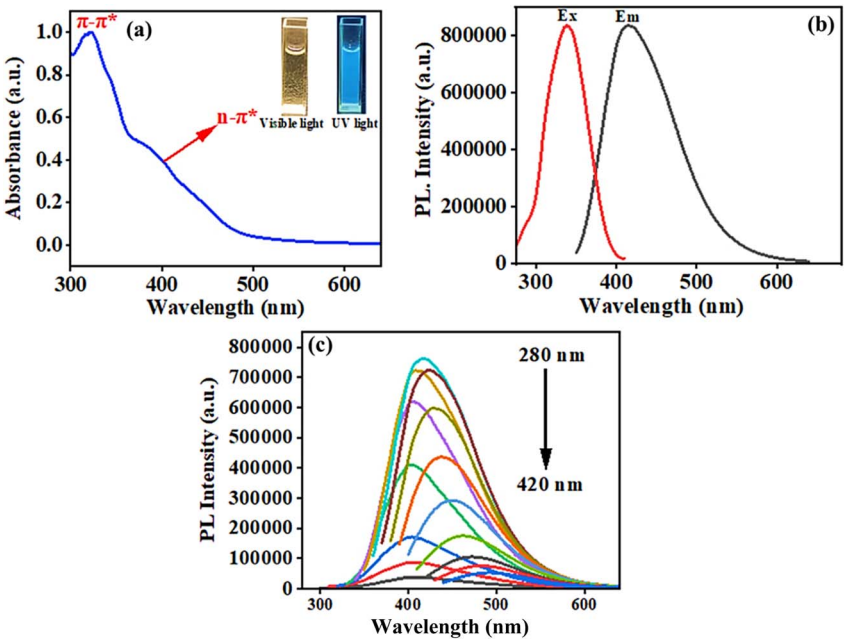

Fig. 3 (a) UV-vis absorption spectrum of CDs with inset images showing fluorescence under visible and 365 nm UV illumination. (b) Excitation and emission spectra of the CDs. (c) Changes in fluorescence emission spectra of CDs showing excitation-dependent photoluminescence spectra in the range of λ_{ex}: 280 nm to 430 nm, highlighting excitation-tunable emission.

their fluorescence intensity. The as-synthesized CDs exhibited an initial pH of 9, reflecting their highly alkaline nature, owing to surface hydroxyl (–OH) groups. The pH-dependent fluorescence response arises primarily from protonation and deprotonation of these surface functional groups. Increasing the pH from 9 to 12 caused a significant decrease in fluorescence due to deprotonation of –OH and other oxygenated groups, which promotes nonradiative pathways. Conversely, under acidic conditions (pH 3–9), protonation stabilizes the surface states and induces electrostatic repulsion between CDs, mitigating aggregation and enhancing emission intensity. (Fig. S2a). The reversible pH-dependent fluorescence of CDs arises from protonation-deprotonation of surface functional groups, which modulates their emissive states. This intrinsic responsiveness enables N-CDs to serve as sensitive and reliable pH probes, offering significant promise for biological and environmental applications.[43] The negligible effect of ionic strength (0–100 mM NaCl) on fluorescence indicates that the photoluminescence is primarily governed by intrinsic surface states rather than external electrostatic screening, highlighting the robustness of the CDs in complex environments. The influence of ionic strength was further assessed by titrating NaCl (0–100 mM) into the CD dispersion. The fluorescence intensity remained largely unaffected, indicating the CDs' remarkable robustness and stability even under high ionic strength conditions (Fig. S2b).

3.3.2 Impact of photostability and storage stability on the performance of CDs. For a nanosensor to be practically effective, both photostability and chemical stability are essential parameters, particularly for the reliable detection of metal ions and bioactive molecules. The CDs demonstrated remarkable photostability, with their fluorescence intensity remaining essentially unchanged under continuous irradiation from a 150 W xenon arc lamp for 60 min (Fig. S2c). Long-term storage stability was further confirmed by monitoring fluorescence over 60 days, with measurements taken every 10 days, revealing no appreciable loss of emission intensity (Fig. S2d). These results collectively underscore the CDs excellent stability, highlighting their suitability for real-world sensing applications.

3.4 Assessment of selectivity and interference performance of the nanosensor

Selectivity is a critical parameter in the design of effective nanosensors. To evaluate this, the fluorescence response of the as-prepared CDs was examined in the presence of various potential interferents, including metal ions, amino acids, and bioactive molecules. A 1 mM concentration of metal ions (K^+, Mg^{2+}, Ni^{2+}, NH_4^+, Cu^+, Pb^{2+}, Ba^{2+}, Mn^{2+}, Cr^{2+}, Na^+; Fig. 4a) and amino acids (Ala, Arg, Asn, Asp, Glu, His, Ile, Leu, Lys, Met, Thr, Val; Fig. 4b) produced negligible changes in fluorescence intensity. Similarly, most bioactive molecules, such as ascorbic acid, creatinine, dopamine, and tetracycline, had minimal effect, whereas quercetin and riboflavin induced significant quenching of the photoluminescence (Fig. 4c). This selective response is likely governed by specific quenching mechanisms associated with these antioxidants. These results establish the CDs as highly selective and practical fluorescent probes for detecting antioxidant molecules, such as quercetin (QT) and riboflavin (RF).

3.5 Fluorescence sensitivity of CDs toward QT and riboflavin RF

High selectivity and sensitivity are indispensable characteristics for nanosensors intended for practical applications. The

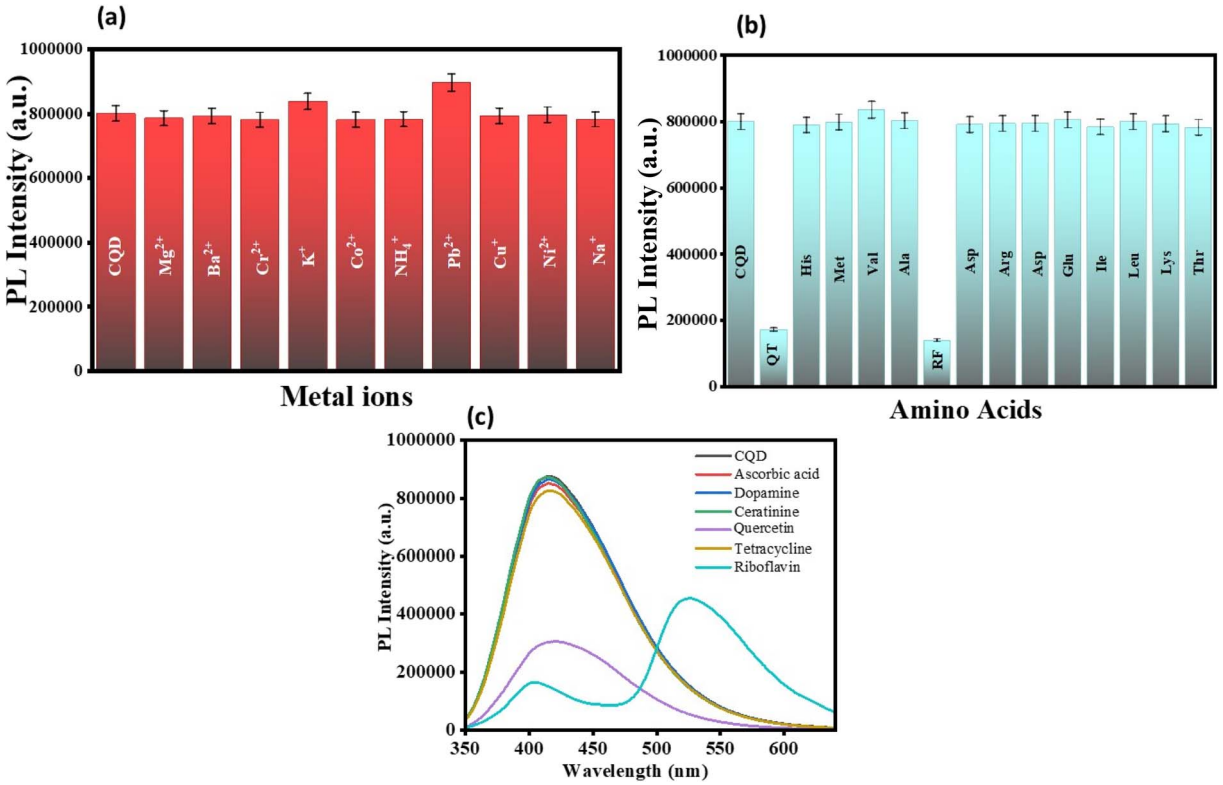

Fig. 4 Fluorescence emission response of selectivity studies of CDs with (a) metal ions, (b) amino acids, and (c) bioactive molecules, highlighting selective quenching by quercetin (QT) and riboflavin (RF).

sensitivity of the CDs toward quercetin (QT) was systematically evaluated under optimized conditions, wherein 10 μL of the CDs stock solution was diluted in 3 mL of water to prepare a working dispersion, followed by incremental addition of QT aliquots at varying concentrations. A progressive decrease in fluorescence intensity (Fig. 5a) was observed with increasing QT concentration (0–19.6 μM), confirming concentration-dependent quenching of the CDs. To quantitatively assess the quenching behavior, the Stern–Volmer relationship was applied, and the corresponding plot was constructed according to the following equation:[34]

$$\frac{F_0}{F} = 1 + K_{SV}[\text{quercetin}] \quad (2)$$

where 'F_0' and 'F' represent the fluorescence intensities in the absence and presence of quencher (QT), respectively. A linear correlation between $\frac{F_0}{F}$ and QT concentration was observed in the range of 0 to 20 μM, described by the regression equation $\frac{F_0}{F} = 0.07939X + 0.898$ with $R^2 = 0.97$. The Stern–Volmer quenching constant (K_{SV}) was calculated as 7.9×10^4 M^{-1} (Fig. S3a). Furthermore, using eqn (4), where k refers to the slope of the calibration curve, and σ denotes the standard deviation ($n = 3$), the limit of detection (LOD) for QT was determined to be 0.25 μM with $R^2 = 0.98$ (Fig. 5b). The equation for LOD determination is given below:[3]

$$\text{LOD} = \frac{3\sigma}{k} \quad (3)$$

Analogous to QT, the sensitivity of CDs toward riboflavin (RF) was investigated using fluorescence quenching assays. A stock solution of RF was prepared, and a working dispersion of CDs was obtained by diluting 10 μL of the CDs stock solution in 3 mL of deionized water. Subsequently, incremental aliquots of RF at varying concentrations were added to the dispersion, and the resulting fluorescence responses were systematically recorded. A progressive decline in fluorescence quenching was observed, and the quenching efficiency was expressed as the F_0/F ratio, where F_0 and F represent the fluorescence intensities of CDs in the absence and presence of RF, respectively (Fig. 5c). The quenching response followed a polynomial fit ($y = 1.02602 + 0.07922 \times 1 + 0.01168 \times 2$) with a correlation coefficient ($R^2 = 0.97$; Fig. S3b). Furthermore, a well-defined linear response was obtained at lower RF concentrations (1.0–4.5 μM) with $R^2 = 0.99$ (Fig. 5d). The LOD for RF was calculated as 0.14 μM, highlighting the excellent detection sensitivity of CDs toward RF. The prepared nanosensor exhibits high sensitivity to QT and RF, with significantly lower detection limits than previously reported nanosensors in the literature, as summarized in Table 1.

3.6 Evaluation of photophysical parameters

The synthesized CDs exhibited strong blue fluorescence with a PLQY value of ~22.5%. Upon addition of QT and RF, the PLQY values decreased sharply to ~3.2% and ~5.6%, respectively, demonstrating efficient fluorescence quenching toward both analytes (Table S1). Time-correlated single-photon counting (TCSPC) was used to investigate the fluorescence decay of the

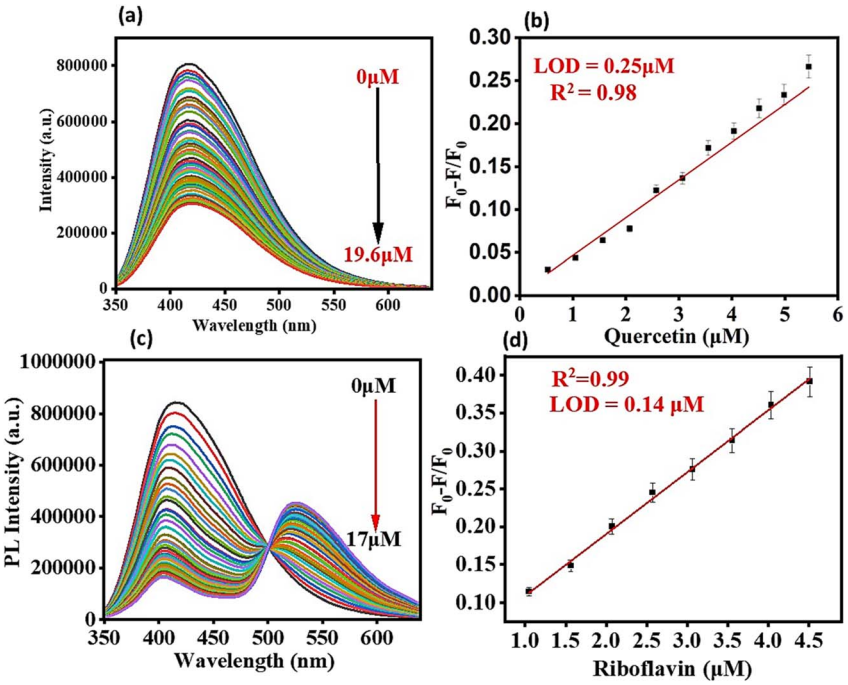

Fig. 5 (a) PL spectra of CDs at different quercetin (QT) concentrations. (b) Linear correlation between $(F_0-F)/F_0$ and QT concentration (0–6 μM) with calculated limit of detection (LOD) value. (c) PL spectra of CDs in the presence of increasing riboflavin (RF) concentrations. (d) Linear correlation between $(F_0-F)/F_0$ and RF concentration (1–4.5 μM) calculated LOD value. Error bars denote the standard error of measurements derived from three independent experiments.

Table 1 Comparative comparison of the suggested approach with previously described literature reports for the detection of quercetin (QT) and riboflavin (RF)

Sensing systems	Linear range (μM)	LOD (μM)	Reference
CDs/quercetin/IFE	10–200 μM	6.41	44
CQDs/quercetin/FET	20–90 μM	6.73	45
ZnSQDs/quercetin/static quenching	2.65–7.5 μM	5.71×10^{-7}	46
Mn doped ZnSQDs/quercetin/interaction mechanism	0.1–6 mg L^{-1}	0.047 mg L^{-1}	47
Biomass-derived carbon dots/quercetin	1–60 μM	0.42 μM	48
Fluorescent carbon dots (green synthesis)/quercetin	2–80 μM	0.31 μM	49
CDs modified with DES/quercetin/IFE	0–20 μM	0.25 μM	Present work
NPCDs/riboflavin/FRET	0.5–50 μM	0.17 μM	50
Graphitic carbon nitride/riboflavin/FRET	0.4–10 μM	0.17 μM	51
Carbon dots/FRET	0.5–20 μM	0.18 μM	52
Fluorescent polymer probe/FRET	0.2–50 μM	0.20 μM	53
Quantum dot-based sensor/FRET	1–100 μM	0.25 μM	54
CDs modified with DES/FRET/riboflavin	1.0–4.5 μM	0.14 μM	Present work

CDs in the presence of the analytes. The average fluorescence lifetime (τ_{avg}) was determined to be 2.93 ns. In the presence of QT, no significant change in τ_{avg} (2.85 ns) was observed, whereas a pronounced decrease in τ_{avg} to 2.10 ns was recorded upon addition of RF. These TCSPC results (Table S1) indicate that QT and RF interact with the CDs through distinct quenching mechanisms.

3.7 Plausible mechanistic elucidation of fluorescence quenching between CDs and QT

Interactions between CDs and fluorophores can modulate emission behavior through multiple quenching pathways, including the inner filter effect (IFE), photoinduced electron transfer (PET), Förster resonance energy transfer (FRET), and dynamic or static quenching. To elucidate the fluorescence quenching mechanism governing quercetin (QT) detection, the interaction between QT and CDs was systematically examined. A pronounced spectral overlap between the absorption spectrum of QT and the emission spectrum of CDs was observed (Fig. 6a), with absorption and emission maxima at 366 and 417 nm, respectively, indicating the possible involvement of IFE or FRET. Time-resolved fluorescence measurements showed no appreciable change in the average lifetime of CDs upon QT addition (Fig. 6b and Table S1), thereby excluding dynamic quenching pathways. Further support was obtained from

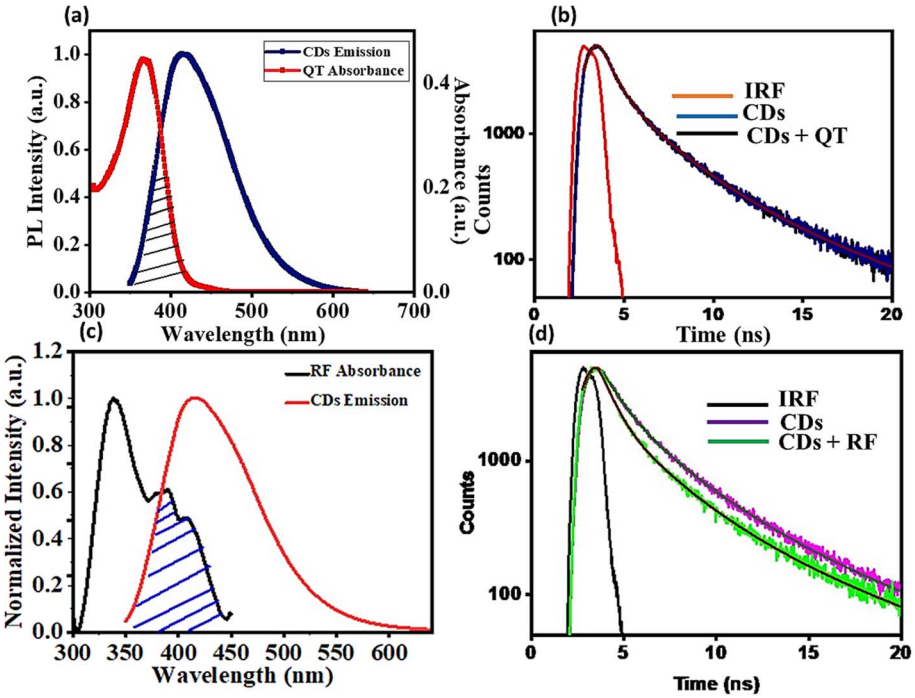

Fig. 6 (a) Overlap spectra of absorption spectrum of quercetin (QT) with emission spectrum of CDs. (b) Fluorescence lifetime decay of CDs in presence of QT, (c) Overlap of absorption spectrum of riboflavin (RF) with emission spectrum of CDs. (d) Fluorescence lifetime decay of CDs in presence of RF.

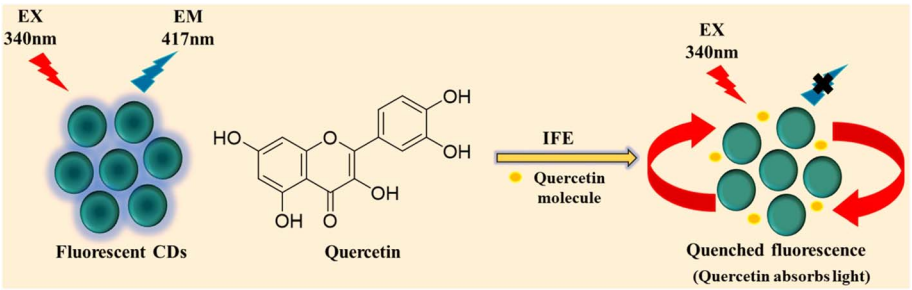

Scheme 2 A schematic representation of the inner filter effect (IFE)-based fluorescence quenching process involving carbon dots (CDs) and quercetin (QT). CDs emit fluorescence at 417 nm after being excited at 340 nm; however, in the presence of QT, spectral overlap causes QT to absorb emission light, resulting in attenuated (quenched) fluorescence intensity.

dilution experiments, wherein incremental addition of deionized water to a solution containing CDs and QT resulted in a progressive recovery of fluorescence intensity (Fig. S3d), a hallmark of IFE-driven attenuation. Zeta potential measurements revealed negative surface charges for both CDs (−4.23 mV) and QT (−2.81 mV) (Fig. S3c), suggesting limited electrostatic interaction between the two species. Notably, the addition of QT induced a shift of the CDs zeta potential toward positive values (Fig. S3c), indicating some degree of interaction between the two species and providing supportive evidence consistent with the proposed quenching mechanism. Collectively, these results indicate that the inner filter effect is the dominant mechanism responsible for QT-induced fluorescence quenching of CDs, as schematically illustrated in Scheme 2.[3,38]

3.8 Plausible mechanistic elucidation of fluorescence quenching between CDs and RF

Addition of riboflavin (RF, 0–17 μM) to carbon dots (CDs) induced a concentration-dependent quenching of CD fluorescence (Fig. 5c). The substantial overlap between the CD emission and RF excitation spectra (Fig. 6c) meets the spectral requirements for Förster resonance energy transfer (FRET). Zeta potential measurements confirmed that both CDs and RF remain negatively charged before and after mixing (Fig. S4a), excluding electrostatic association or ground–state complex formation. Dilution experiments showed no fluorescence recovery upon addition of deionized water (Fig. S4b), ruling out inner filter effects. Consistently, time-correlated single-photon counting revealed a marked decrease in the average

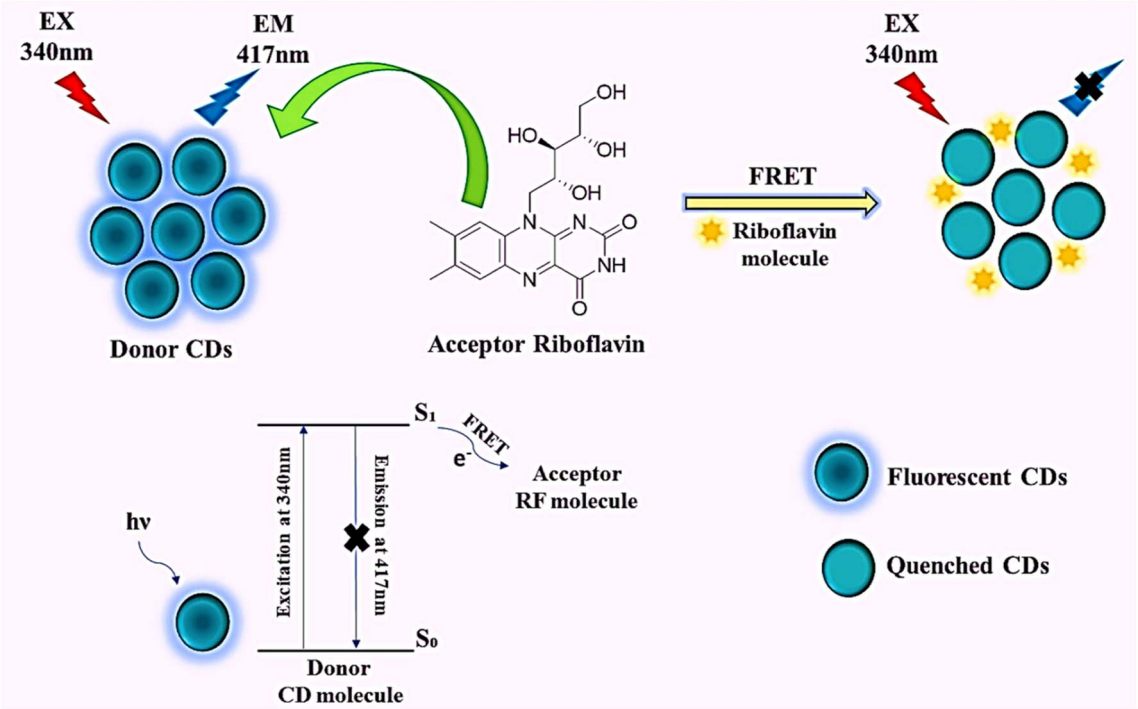

Scheme 3 Schematic representation of the Förster resonance energy transfer (FRET) process involving carbon dots (CDs) and riboflavin (RF), in which CDs thrive as energy donors (λ_{ex} 340 nm, λ_{em} 417 nm) and transfer energy to RF as the acceptor *via* spectral overlap, resulting in CDs' fluorescence being quenched.

fluorescence lifetime of CDs in the presence of RF (Fig. 6d and Table S1). These results conclusively identify the FRET mechanism[38] governing RF-induced fluorescence quenching of CDs (Scheme 3).[29]

To further substantiate the proposed Förster resonance energy transfer (FRET) mechanism between the CDs and RF, the spectral overlap integral [$J(\lambda)$] was quantitatively evaluated from the overlap between the normalized emission spectrum of CDs (donor) and the excitation spectrum of RF (acceptor) according to the following expression:[34]

$$J(\lambda) = \frac{\int_0^\infty F_D(\lambda)\varepsilon_A(\lambda)\lambda^4 d\lambda}{\int_0^\infty F_D(\lambda)d\lambda} \quad (4)$$

'F_D (λ)' denotes the normalized fluorescence emission intensity of the donor at wavelength λ, and 'ε_A' corresponds to the molar extinction coefficient of the acceptor at the same wavelength. Furthermore, the Förster distance (R_0) (eqn (5), defined as the donor–acceptor separation at which the energy transfer efficiency is 50%, was calculated using the following expression:[34]

$$R_0 = 0.211[\kappa^2\eta^{-4}\Phi_D J(\lambda)]^{1/6} \quad (5)$$

The orientation factor 'κ^2' describes the relative alignment of the donor and acceptor transition dipole moments; for randomly oriented dipoles in an isotropic solution, κ^2 was assumed to be 2/3. The term η represents the refractive index of the medium, and Φ_D denotes the fluorescence quantum yield of the donor. For the CDs-RF system in an aqueous medium, the Förster distance (R_0) was determined to be 3.51 nm (Table S1b). This value, being well below 10 nm, satisfies the fundamental criterion of classical Förster theory, which requires nanometer-scale donor–acceptor separation for efficient nonradiative energy transfer. The calculated R_0 value, therefore, supports the occurrence of effective FRET between CDs and RF under the present experimental conditions.

Further, electron transfer rate (k_{ET}) was determined using the following equation:[34]

$$k_{ET} = \frac{1}{\tau_{DA}} - \frac{1}{\tau_D} \quad (6)$$

The parameters 'τ_{DA}' and 'τ_D' represent the average excited-state lifetimes of CDs in the presence and absence of RF, respectively. The calculated 'k_{ET}' value (Table S1b) confirms the occurrence of an electron transfer process between CDs and RF. Furthermore, to elucidate the nature of the interaction, the Förster resonance energy transfer (FRET) efficiency of the CD–RF nanosensor system was determined using eqn (7) and found to be 21.4% (Table S1b), supporting an electron-transfer–dominated quenching mechanism.[34]

$$E = \frac{k_{ET}}{k_r + k_{ET} + k_{nr}} \quad (7)$$

Additionally, the donor–acceptor separation distance (r) between CDs and riboflavin RF was estimated from the calculated FRET efficiency using the standard Förster relation:[34]

$$E = \frac{1}{1 + \left(\frac{r}{R_0}\right)^6} \quad (8)$$

The interparticle distance (r) was determined to be 4.36 nm (Table S1b), which falls within the effective Förster distance (<10 nm), thereby confirming that the CDs and RF are sufficiently close to facilitate resonance energy transfer.

3.9 Real sample quantification of QT in apple juice

To assess the practical utility of the developed sensing platform, QT was quantified in apple juice using a standard-addition (spike-recovery) method. Fresh apples obtained from a local market were peeled, homogenized, and filtered to afford freshly prepared juice, which was used without further treatment. Aliquots of QT at known concentrations were spiked into the sample, and fluorescence measurements were conducted under identical experimental conditions. In the apple juice matrix, the LOD value was determined to be ~0.43 μM (Fig. S5a). The CDs enabled reliable quantification of QT in the micromolar regime, affording satisfactory recoveries with low relative standard deviation (RSD) values (Table S2). These findings substantiate the accuracy, reproducibility, and practical applicability of the proposed sensing methodology in complex sample matrices.

3.10 Real sample quantification of RF in vitamin B_2 tablets

To validate the practical applicability of the developed nanosensor, RF was quantified in commercially available vitamin B_2 tablets using a standard addition protocol. The tablet samples were appropriately processed and analyzed under identical experimental conditions. In the real sample matrix, the LOD value was determined to be ~0.66 μM (Fig. S5b). The synthesized carbon dots enabled sensitive detection of RF in the micromolar range, affording satisfactory recovery values with low relative standard deviation (RSD) (Table S3). These results confirm the robustness, accuracy, and suitability of the proposed sensing platform for the determination of riboflavin in pharmaceutical formulations.

4 Conclusions

Carbon dots (CDs) were synthesized from a renewable biomass precursor (clove) and surface-engineered using a deep eutectic solvent (DES) composed of choline chloride and urea (1 : 1 molar ratio). This straightforward, rapid, and cost-effective hydrothermal strategy afforded highly fluorescent CDs with a quantum yield of ~22.5%. The nanodots exhibited pronounced photostability, excitation-dependent emission behavior, and excellent environmental stability. Structural and surface chemical analyses (EDS, XPS, and FTIR) confirmed successful functionalization, while HRTEM revealed uniformly dispersed nanoparticles with an average diameter of 2.1 nm. The prepared CDs served as a dual-analyte fluorescent nanosensor with high selectivity for quercetin (QT) and riboflavin (RF) *via* distinct quenching pathways. QT-induced fluorescence attenuation was governed predominantly by the inner filter effect (IFE), whereas riboflavin-mediated quenching proceeded *via* a Förster resonance energy transfer (FRET) mechanism. The limits of detection were 0.25 μM for QT and 0.14 μM for RF. Upon analyte interaction, the quantum yield of the CDs decreased to 3.2% (QT) and 5.6% (RF), consistent with efficient excited-state deactivation. Relative to conventional synthetic approaches, the present methodology offers advantages in sustainability, operational simplicity, reduced reaction time, and economic feasibility. The developed platform demonstrates significant potential for applications in biochemical analysis, environmental monitoring, and medicinal chemistry, providing a versatile and efficient system for detecting biologically relevant antioxidants. The conclusion section should not just be informative like the abstract. It should more effectively highlight the research achievements of the demonstrated study.

Conflicts of interest

The authors affirm that they have no known financial or interpersonal conflicts that would have appeared to have an impact on the research presented in this study.

Data availability

All data supporting the findings of this study are available within the article and its supplementary information (SI). Supplementary information: Fig. S1 depicts (a) optimization of CDs concentration, (b) reaction time-dependent optimization of CDs synthesis, and (c) the EDS spectrum of the as-prepared CDs; Fig. S2 shows (a) the effect of pH, (b) the effect of ionic strength, (c) photo irradiation studies, and (d) storage studies on the prepared CDs; Fig. S3 illustrates the Stern–Volmer plot between F_0/F and different concentrations of (a) QT and (b) RF, along with (c) zeta potential of CDs, QT, and CDs + QT, and (d) the effect of dilution on QT; Fig. S4 presents (a) zeta potential of CDs, RF, and CDs + RF and (b) the effect of dilution on RF; Fig. S5 shows (a) the linear relationship of F_0/F of carbon dots with different concentrations of QT in a real apple juice sample and (b) the linear correlation of F_0/F with different concentrations of RF in a real vitamin B_2 tablet sample; Table S1 summarizes (a) photophysical parameters of CDs in the presence of analytes and (b) FRET parameters of CDs in the presence of RF; Table S2 presents real estimation of QT in apple juice; and Table S3 presents real estimation of RF in vitamin B_2 tablets. See DOI: https://doi.org/10.1039/d6ra02145j.

Acknowledgements

We gratefully acknowledge financial assistance from the Anusandhan National Research Foundation (ANRF) for the SRG grant to B. M. (SRG/2022/000942). We are also grateful to CIL, Punjab University, Chandigarh, for the HR-TEM analysis; CRF, IIT Roorkee, for the XPS analysis; and TIET Patiala for the EDS

analysis facility. We also acknowledge the research facility at TIET-VT CEEMS for the FTIR analysis, and Dr Bhupendra Kumar Chudasama, professor, SPMS, TIET, Patiala, for his kind permission for the zeta potential analysis. AI-assisted writing tools (ChatGPT, Grammarly, and QuillBot) were used only for language polishing and grammar checks.

References

1 T. El Achkar, H. Greige-Gerges and S. Fourmentin, *Environ. Chem. Lett.*, 2021, **19**, 3397–3408, DOI: 10.1007/s10311-021-01225-8.
2 Y. Ma, Y. Yang, T. Li, S. Hussain and M. Zhu, *Green Chem.*, 2024, **26**, 3627–3669, DOI: 10.1039/D3GC04289H.
3 M. Kaur, M. Bhattacharya and B. Maity, *RSC Adv.*, 2025, **15**, 19884–19898, DOI: 10.1039/D5RA00824G.
4 C. Florindo, F. Lima, B. D. Ribeiro and I. M. Marrucho, *Curr. Opin. Green Sustain. Chem.*, 2019, **18**, 31–36, DOI: 10.1016/j.cogsc.2018.12.003.
5 O. Długosz and M. Banach, *J. Clean. Prod.*, 2024, **434**, 139914, DOI: 10.1016/j.jclepro.2023.139914.
6 F. Zannat, M. A. Alam, P. Ghosh, R. K. Bishwas and S. A. Jahan, *Mater. Adv.*, 2025, **6**, 8431–8447, DOI: 10.1039/D5MA01083G.
7 P. Zhao, X. Li, G. Baryshnikov, B. Wu, H. Ågren, J. Zhang and L. Zhu, *Chem. Sci.*, 2018, **9**, 1323–1329, DOI: 10.1039/C7SC04607C.
8 D. Gömpel, M. N. Tahir, M. Khan, S. F. Adil, M. R. Shaik, M. Kuniyil, A. Al-Warthan and W. Tremel, *Dalton Trans.*, 2024, **53**, 3132–3142, DOI: 10.1039/d3dt02605a.
9 S. Ponce, M. Hernandez, K. Vizuete, D. A. Streitwieser and A. Debut, *Colloid Interface Sci. Commun.*, 2021, **43**, 100457, DOI: 10.1016/j.colcom.2021.100457.
10 J. S. Lee, *Nanotechnol. Rev.*, 2017, **6**, 271–278, DOI: 10.1515/ntrev-2016-0106.
11 H. E. Emam, *Carbohydr. Polym.*, 2024, **324**, 121503, DOI: 10.1016/j.carbpol.2023.121503.
12 M. Phull, A. Ali and B. Maity, *RSC Sustain.*, 2024, **2**, 1599–1612, DOI: 10.1039/D4SU00004H.
13 S. A. Hira, S. Durairaj, C. A. Ramirez and A. Chen, *Nanoscale*, 2025, **17**, 27762–27783, DOI: 10.1039/D5NR03879K.
14 A. K. Pandey, T. K. Nath and S. Dhara, *Colloids Surf., B*, 2022, **220**, 441–455, DOI: 10.1016/j.jiec.2024.07.006.
15 M. Pan, X. Xie, K. Liu, J. Yang, L. Hong and S. Wang, *Nanomater*, 2020, **10**, 930, DOI: 10.3390/nano10050930.
16 J. V. Kumar and J. W. Rhim, *J. Environ. Chem. Eng.*, 2024, **12**, 111999, DOI: 10.1016/j.jece.2024.111999.
17 J. M. Fernández-Romero and M. P. Aguilar-Caballos, *Fluoresc*, 2019, **3**, 281–291, DOI: 10.1016/B978-0-12-409547-2.00156-6.
18 M. J. Molaei, *Talanta*, 2019, **196**, 456–478, DOI: 10.1016/J.TALANTA.2018.12.042.
19 B. Wang and S. Lu, *Matter*, 2022, **5**, 110–149, DOI: 10.1016/j.matt.2021.10.016.
20 J. Wu, X. Yue, T. Wang, Y. Zhang, Y. Jin and G. Li, *Colloids Surf., A*, 2025, **717**, 136850, DOI: 10.1016/j.colsurfa.2025.136850.
21 Z. Zhan, J. Zhang, L. Lin, T. Jiang and J. Shi, *Ind. Crop. Prod.*, 2025, **236**, 122105, DOI: 10.1016/j.indcrop.2025.122105.
22 H. Zhu, M. Hu, Y. Zhang, A. Abudurahman, Y. Zhu and J. Cui, *Fuel*, 2026, **410**, 137855, DOI: 10.1016/j.fuel.2025.137855.
23 M. Phull, A. Ali, J. Brar, A. Mishra and B. Maity, *Nanoscale*, 2026, **18**, 1560–1575, DOI: 10.1039/D5NR03407H.
24 S. Roy, N. Preeyanka, D. Majhi, S. Seth and M. Sarkar, *J. Phys. Chem. C*, 2018, **122**, 12384–12394, DOI: 10.1021/acs.jpcc.8b03859.
25 N. Ngafwan, H. Rasyid, E. Salaam Abood, W. Kamal Abdelbasset, S. G. Al-Shawi, D. Bokov and A. T. Jalil, *Food Sci. Technol.*, 2022, **42**, e37821, DOI: 10.1590/fst.37821.
26 C. Zehiroglu and S. B. Ozturk Sarikaya, *J. Food Sci. Technol.*, 2019, **56**, 4757–4774, DOI: 10.1007/s13197-019-03952-x.
27 A. Jeevika, G. Alagarsamy and J. Celestina, *J. Lumin.*, 2022, **37**, 1991–2001, DOI: 10.1002/bio.4381.
28 S. Momeni, A. M. Ramezani, S. Talebi and I. Nabipour, *J. Food Compos. Anal.*, 2023, **120**, 105296, DOI: 10.1016/j.jfca.2023.105296.
29 M. Kaur, M. Bhattacharya and B. Maity, *RSC Sustain.*, 2024, **2**, 1472–1486, DOI: 10.1039/D3SU00456B.
30 G. Muthusankar, C. Rajkumar, S. M. Chen, R. Karkuzhali, G. Gopu, A. Sangili, N. Sengottuvelan and R. Sankar, *Sens. Actuators, B*, 2019, **281**, 602–612, DOI: 10.1016/j.snb.2018.10.145.
31 K. Halicka, F. Meloni, M. Czok, K. Spychalska, S. Baluta, K. Malecha, M. I. Pilo and J. Cabaj, *ACS Omega*, 2022, **7**(38), 33749–33768, DOI: 10.1021/acsomega.2c04134.
32 Y. Tang, S. Shang, J. Yang, B. Lü, F. Peng, W. Huan and J. Bian, *Ind. Crop. Prod.*, 2025, **224**, 120440, DOI: 10.1016/j.indcrop.2024.120440.
33 S. Khare, N. Sohal, M. Kaur and B. Maity, *Heliyon*, 2025, **11**, e41853, DOI: 10.1016/j.heliyon.2025.e41853.
34 J. R. Lakowicz, *Principles of Fluorescence Spectroscopy*, Springer, Boston, 2006, DOI: 10.1007/978-0-387-46312-4.
35 A. A. Sa, A.-H. Fa, A. G. Al-Kaf, T. Al-Deen, S. Ahmed, A. Alhaidrai and S. A. Ali Alhaidrai, *Bioequiv. Bioavail. Int. J.*, 2022, **6**, 2578–4803, DOI: 10.23880/beba-16000179.
36 Z. Hu, X. Y. Jiao and L. Xu, *Microchem. J.*, 2020, **154**, 104588, DOI: 10.1016/j.microc.2019.104588.
37 W. Tang, P. Li, G. Zhang, X. Yang, M. Yu, H. Lu and X. Xing, *J. Appl. Polym. Sci.*, 2021, **138**, 50620, DOI: 10.1002/app.50620.
38 C. Yu, D. Qin, X. Jiang, X. Zheng and B. Deng, *J. Pharm. Biomed. Anal.*, 2020, **192**, 113673, DOI: 10.1016/j.jpba.2020.113673.
39 H. L. Yang, L. F. Bai, Z. R. Geng, H. Chen, L. T. Xu, Y. C. Xie, D. J. Wang, H. W. Gu and X. M. Wang, *Mater. Today Adv.*, 2023, **18**, 100376–100400, DOI: 10.1016/j.mtadv.2023.100376.
40 S. E. Elugoke, G. E. Uwaya, T. W. Quadri and E. E. Ebenso, *ACS Symposium Series*, 2024, vol. 1465, pp. 3–42, DOI: 10.1021/bk-2024-1465.ch001.
41 A. B. Siddique, S. M. Hossain, A. K. Pramanick and M. Ray, *Nanoscale*, 2021, **13**, 16662–16671, DOI: 10.1039/D1NR04301C.

42 W. You, W. Zou, S. Jiang, J. Zhang, Y. Ge, G. Lu, D. W. Bahnemann and J. H. Pan, *Carbon Neutralization*, 2023, **3**, 245–284, DOI: 10.1002/cnl2.120.
43 Y. Liu, M. Fang, Z. Wu, H. Wang, Y. Li, C. Dong, S. Shuang and X. Gong, *Spectrochim. Acta, Part A Mol. Biomol. Spectrosc.*, 2025, **333**, 125868, DOI: 10.1016/j.saa.2025.125868.
44 J. Wang, D. Han and Z. Yan, *Spectrosc. Lett.*, 2024, **57**, 428–441, DOI: 10.1080/00387010.2024.2370816.
45 A. Jeevika, G. Alagarsamy and J. Celestina, *J. Lumin.*, 2022, **37**, 1991–2001, DOI: 10.1002/BIO.4381.
46 D. Wu and Z. Chen, *Lumin*, 2014, **29**, 307–313, DOI: 10.1002/BIO.2545.
47 Z. Zhang, Y. Miao, L. Lian and G. Yan, *Anal. Biochem.*, 2015, **489**, 17–24, DOI: 10.1016/J.AB.2015.08.002.
48 C. Xu, B. Wang, J. Xing, Y. Zhao, L. Zhu, J. Zhang, B. Wei and H. Wang, *New J. Chem.*, 2024, **48**, 16631–16641, DOI: 10.1039/D4NJ02578D.
49 J. Wang, D. Han and Z. Yan, *Spectrosc. Lett.*, 2024, **57**, 428–441, DOI: 10.1080/00387010.2024.2370816.
50 L. Lin, Y. Wang, Y. Xiao and X. Chen, *Anal. Bioanal. Chem.*, 2019, **411**, 2803–2808, DOI: 10.1007/S00216-019-01725-1.
51 J. Han, H. Y. Zou, M. X. Gao and C. Z. Huang, *Talanta*, 2016, **148**, 279–284, DOI: 10.1016/j.talanta.2015.10.038.
52 X. Wu, F. Tian, W. Wang, J. Chen, M. Wu and J. B. Zhao, *Sens. Actuators, B*, 2017, **241**, 1040–1046, DOI: 10.1016/j.snb.2016.10.121.
53 X. Chen, T. Pradhan, F. Wang, J. S. Kim and J. Yoon, *Talanta*, 2018, **182**, 69–77, DOI: 10.1016/j.talanta.2018.01.052.
54 Y. Zhang, J. Zhao and G. Chen, *Anal. Chim. Acta*, 2019, **1052**, 131–137, DOI: 10.1016/j.aca.2018.11.046.